The effects of nitrate on the heterogeneous uptake of sulfur dioxide on hematite

L. D. Kong, X. Zhao, Z. Y. Sun, Y. W. Yang, H. B. Fu, X. Yang, S. C. Zhang, J. M. Chen, L. Wang, and T. T. Cheng

Shanghai Key Laboratory of Atmospheric Particle Pollution and Prevention, Department of Environmental Science & Engineering, Fudan University, Shanghai 200433, China

Lingdong Kong: ldkong@fudan.edu.cn (corresponding author)

Abstract. Nitrate is often found to be associated with atmospheric particles. Surface nitrate can change the hygroscopicity of these particles, and thus impact their chemical reactivity. However, the influence of nitrate on heterogeneous reactions of atmospheric trace gases is poorly understood. In this work, the effects of nitrate on heterogeneous conversion of SO_2 with hematite at 298 K are investigated using an in situ diffuse reflectance infrared Fourier transform spectroscopy (DRIFTS) and a White cell coupled with Fourier transform infrared spectroscopy (White cell-FTIR). It is found that nitrate participates in heterogeneous reactions of SO_2, accelerates the formation rate of sulfate, and leads to the formation of surface-adsorbed HNO_3 and gas-phase N_2O and HONO. The results indicate that low to moderate amounts of nitrate significantly enhance the reactivity of hematite-nitrate mixtures, the uptake of SO_2 and the formation of sulfate on hematite. For mixtures, the sample containing 24% nitrate exhibits the highest sulfate formation rate, and its corresponding uptake coefficient calculated by geometric surface area is about 5.5 times higher than that of hematite alone. The sample containing 48% nitrate presents the highest BET uptake coefficient, and the value is about 8 times higher than that of pure hematite. No uptake of SO_2 and formation of sulfate are observed on pure nitrate. Evidence presented herein implies a significant contribution of the unreleased HNO_3 and HONO in the particles for the conversion of SO_2 and the enhanced formation of sulfate in the atmosphere. A possible mechanism for the influence of nitrate on the heterogeneous conversion of SO_2 on hematite is proposed, and atmospheric implications based on these results are discussed.

1 Introduction

Sulfur dioxide is a major component of air pollution. It is usually generated by the combustion of fossil fuels and by the atmospheric oxidation of biogenic organic sulfur compounds, particularly dimethyl sulfide. The oxidation of sulfur dioxide leads to sulfate particulate formation. Atmospheric sulfate particles play significant roles in adverse health effects, visibility degradation and rain water acidification (Seinfeld and Pandis, 2006). The conversion of SO_2 to sulfate in the atmosphere usually occurs via three well-known pathways, including gas-phase oxidation to sulfuric acid followed by condensation into the particulate-phase, aqueous-phase oxidation in cloud and fog droplets, and various heterogeneous reactions on the surfaces of aerosol particles (Kerminen et al., 2000). There have been a number of atmospheric chemistry models applied to predict the formation of sulfate aerosols on a global scale (Kasibhatla et al., 1997; Laskin et al., 2003). The results suggest that atmospheric SO_2 concentrations are typically overestimated while sulfate concentrations tend to be underestimated (Kasibhatla et al., 1997; Laskin et al., 2003), and the two pathways including gaseous oxidation by OH radical and aqueous oxidation in cloud and fog droplets by ozone and hydrogen peroxide are insufficient to bridge the gap between field and modeling studies (Luria and Sievering, 1991). Including in-cloud oxidation catalyzed by natural transition metal ions in models will improve agreement between models and observations (Harris et al., 2013). These imply that the heterogeneous conversion of SO_2 to sulfate on aerosols may make an important contribution to the atmospheric sulfate concentration, or there are some unknown pathways for the formation of sulfate in the troposphere. The heterogeneous oxidation of SO_2 to sulfate on aerosols has therefore received increasing

attention in recent years. To date there have been a lot of studies regarding heterogeneous reactions of SO_2 on various model oxides and mineral dust particles (Dentener et al., 1996; Goodman et al., 2001; Usher et al., 2002; Ullerstam et al., 2003; Baltrusaitis et al., 2007; Lin et al., 2010; Zhu et al., 2011; Wu et al., 2011; Liu et al., 2012). However, the atmospheric heterogeneous reactions of SO_2 still have large uncertainties (Laskin et al., 2003), and the underlying mechanisms of sulfate formation on mineral aerosols are not completely understood (Dentener et al., 1996). For example, in the atmosphere, the heterogeneous reactions of SO_2 are unavoidably affected by other atmospheric species, but little attention has been paid to the effects of other species on the heterogeneous reaction of SO_2 in the laboratory studies up to now (Ullerstam et al., 2003; Lin et al., 2010; Wu et al., 2011; Liu et al., 2012).

Mineral dust aerosol, emitted from the arid and semiarid regions with a global source strength of about 1000-3000 Tg yr^{-1}, is one of the most important contributors to the airborne particulate matter (Dentener et al., 1996). It is now widely recognized that mineral dust aerosols provide reactive surfaces for atmospheric trace gases, and the reactions on mineral dust particles change their sizes, optical and hygroscopic properties as well as lifetime in the atmosphere, which, in turn, can change the climate impact of these particles. Mineral oxide represents an important and reactive component of mineral dust aerosol. Being one of the typical oxide minerals, Fe_2O_3 contributes ~6% by mass to the total dust burden in the atmosphere (Usher et al., 2003). Atmospheric chemical processing of Fe-containing dust particles during long-range transport can impact the amount of soluble iron (Zhuang et al., 1992; Meskhidze et al., 2003), while soluble iron will limit phytoplankton primary productivity in extensive regions of the ocean referred

to as high-nutrient low-chlorophyll regions (Moore et al., 2002), which ultimately has implications for global climate as well as carbon and nitrogen cycles (Jickells and Spokes, 2001). Thus, there is interest in the atmospheric chemistry of Fe_2O_3. On the other hand, field studies have also observed that nitrate is one of the most common components of secondary particles. It's often found to be associated with these mineral dust particles in the atmosphere (Dentener et al., 1996). Surface nitrate enhances hygroscopic properties of original particles and, in turn, changes their physicochemical properties (Hoffman et al., 2004). This will inevitably impact their chemical reactivity, and therefore lead to a remarkable difference in their heterogeneous chemistry. However, little attention has been paid to the influence of nitrate on heterogeneous reactions of SO_2 on atmospheric aerosols up to now (Lin et al., 2010).

In the present study, the effects of nitrate on heterogeneous conversions of SO_2 on mineral particles at room temperature are investigated using an in situ diffuse reflectance infrared Fourier transform spectroscopy (DRIFTS) and a White cell coupled with Fourier transform infrared spectroscopy (White cell-FTIR). Hematite (α-Fe_2O_3, one of the typical components in mineral aerosol) and sodium nitrate (a major form of nitrate in sea-salt particles) were used as model components of particles. The heterogeneous conversion mechanism of SO_2 is proposed and atmospheric implications of the present study are discussed. The results reveal a potential pathway of sulfate formation in the troposphere and the significant contribution of particulate nitrate for the conversion of SO_2 and the enhanced formation of sulfate in the atmosphere.

2 Experimental

2.1 Materials

Hematite was prepared according to the procedure reported previously (Schwertmann and Cornell, 2000). Powder X-ray diffraction confirmed the prepared sample as pure hematite (Fig. S1 in the Supplement). The Brunauer-Emmett-Teller (BET) surface area was 12.1 $m^2 g^{-1}$ (Micromeritics TriStar 3000, Micromeritics Instrument Co., USA.). Sodium nitrate (Analytical grade, Shanghai Ab Chem Co. Ltd.) was used without further purification. Gaseous oxygen, argon (99.999% purity, Shanghai Yunguang Specialty Gases Inc.), and SO_2 (97 ppm, SO_2/N_2, Shanghai Yunguang Specialty Gases Inc.) were introduced through an air-dryer before use.

In order to systematically study the effects of nitrate on heterogeneous reactions of SO_2 with atmospheric aerosols, a series of hematite-sodium nitrate mixtures with the mass fractions of sodium nitrate in the mixtures in the range of 2-90% (w/w) (denoted as FN-2, FN-6, …, FN-90, respectively) were prepared. Hematite was impregnated with a saturated aqueous solution of sodium nitrate, and then the mixtures were stirred manually and dried under an infrared lamp. Considering that aerosol particles in the real atmosphere invariably contain surface-adsorbed water and the surface-adsorbed water plays an important role in the heterogeneous chemistry of atmospheric SO_2, all of the prepared samples were kept in a desiccator at 68% relative humidity (RH) for 48 h before further use. Powder X-ray diffraction indicated that no secondary processes occurred on the hematite surface during the sample preparation and the subsequent sample equilibration (see Fig. S1 in the Supplement). The humid samples including the hematite-nitrate mixtures, pure hematite and nitrate were still loose fine powders after the

equilibration, and this treatment made some adsorbed water molecule layers be present on the samples.

2.2 In situ DRIFTS experiments

In situ DRIFTS spectra were recorded using a Nicolet Avatar 360 FTIR spectrometer, equipped with a high-sensitivity mercury cadmium telluride (MCT) detector and a Spectra-Tech diffuse reflectance accessory, as described previously (Fu et al., 2007; also see Fig. S2 in the Supplement). The DRIFTS sample cell is coupled with a temperature controller. A 30-mg sample was placed into the ceramic sample holder in the in situ chamber, and the sample temperature controller was used to control reaction temperature. Before the reaction gas was introduced, the reaction chamber was purged with argon (100 mL/min) for 1 h, and then a background spectrum of the unreacted powder sample was collected. Subsequently, a mixture of SO_2 (e.g. 3 ppm) and O_2 (21% v/v) with argon carrier was introduced into the chamber at a total flow rate of 100 mL/min, and then IR spectra were collected as a function of reaction time. The total reaction time is about 4-6 h. All spectra reported here were recorded at a resolution of 4 cm^{-1} for 100 scans. All of the measurements were repeated three times. In addition, it should be pointed out that weak surface water loss will be observed during the purge process, but the loss of water is almost stopped after about 40 min. Furthermore, less water loss is also observed after the introduction of the reactive gases. These imply that some water molecules are kept in the sample due to the presence of hygroscopic salt ($NaNO_3$).

2.3 In situ White cell-FTIR experiments

An infrared cell (White cell reactor, Model 19-V, a variable-path long path cell with the optical path length from 2.4 to 24 m. Infrared Analysis, Inc.) coupled to a Fourier transform infrared spectrometer was used to measure trace gaseous reactants and the possible gaseous products formed from the heterogeneous reaction of SO_2. The optical path length was set to the maximum for all of the measurements. The infrared cell was cleaned by ultra-pure water and then dried before every experiment. The infrared cell was connected to a vacuum system and a gas supply system. The apparatus has been described in detail elsewhere (Fu et al., 2007; Zhang et al., 2006; also see Fig. S3 in the Supplement). For in situ FTIR measurements, the experiments were conducted in the absence of light. The infrared cell was flushed with pure argon with the aid of the vacuum system, and this cleaning process was repeated three times before a sample was placed into the infrared cell. A 30-mg sample was placed in a small reaction disc (inner diameter = 1 cm, depth = 0.1 cm) made of quartz, and then the disc was placed into the infrared cell. After the sample was placed, argon was filled into the cell again to 1.01×10^5 Pa, the background spectrum of the gases was collected, and then the infrared cell was evacuated to 20 Pa again. Argon was used as a carrier gas to load the reactive gases SO_2 and O_2 into the infrared cell through the gas supply system. After the infrared cell was filled to a pressure of 1.01×10^5 Pa, it remained at that pressure for 3 min to ensure homogeneous mixing of the gases in the infrared cell before starting to collect the in situ IR spectra. FTIR spectra were recorded using a Nicolet Avatar 360 FTIR equipped with a liquid nitrogen cooled MCT detector. 100 repeat spectral scans were averaged over a range of 600-4000 cm^{-1} at a spectral resolution of 4 cm^{-1}. A single-beam spectrum collected prior to the SO_2 exposure was used as the reference spectrum. In order to trace gaseous

products, a long reaction time (up to 20 h) was adopted in some experiments. The peak areas of the characteristic peaks of SO_2 have a linear correlation with the concentration of SO_2 (R^2 > 0.999). Thus, the concentration of gaseous SO_2 can be determined by measuring the corresponding in situ FTIR spectra peak areas of gaseous SO_2. All of the measurements were repeated at least twice.

2.4 Heterogeneous reaction of SO_2 in the dark

Heterogeneous reactions of SO_2 (50 ppm) on humid hematite, FN-24 and FN-90 were performed in the presence of O_2 (21% v/v) in three 42 mL brown glass bottles in the dark at room temperature for about 3-7 days, respectively. An about 30 mg sample, which was kept in a desiccator at 68% RH for 48 h, was placed flatly on the bottom of the glass bottle, in order to make sure that no sample particles were stuck on the interior wall of glass bottle. Before the reaction gas SO_2 was introduced, a mixture of Ar and O_2 (21% v/v) was introduced into the bottle at a total flow rate of 100 mL/min to expel air from the bottle for an hour, after which the inlet and the outlet of the bottle were closed. Then 2.1 μL of SO_2 (50 ppm) was injected through the septum into the bottle with a microsyringe. After the above treatments, the final amount of water in the bottle should be close to that in the same sample in the DRIFTS cell. The bottle was packed in aluminum foil and then placed in the dark for 3-7 days.

2.5 Ion analysis and N_2O detection

The products formed on the sample surface were analyzed by ion chromatography after DRIFTS experiments. The method is similar to that in a previous study (Ullerstam et al., 2002). The reacted sample particles were extracted by sonication with ultrapure water

200 (specific resistance ≥18.0 MΩ-cm). The leaching solution contained 1% formaldehyde as
201 a preservative to suppress sulfite oxidation and was obtained through a 0.45 μm PTFE
202 membrane filter. The filtered solution was analyzed using a Dionex DX 500 ion
203 chromatography, which was equipped with a Dionex AS 14 analytical column and a
204 CD20 conductivity detector. A weak base eluent (1.0 mM $NaHCO_3$ -3.5 mM Na_2CO_3)
205 was used for anion detection at a flow rate of 1.5 mL/min. Quality assurance of species
206 measurement was routinely carried out by using standard reference materials produced by
207 the National Research Center for Certified Reference Materials, China.

208 A solid phase microextraction-gas chromatography-mass spectrometry (SPME-GC-MS)
209 method was also used to detect nitrous oxide (Drescher et al., 2006). SPME was carried
210 out using a commercial SUPELCO 75 μm Carboxen/PDMS fiber to qualitatively analyze
211 N_2O. Before the fiber was used for the first time, the fiber was conditioned at 280 ℃ until
212 a clean chromatogram was obtained under normal run conditions. In addition, to
213 minimize background signals, the fibers were heated in the GC inlet for 2 to 5 minutes
214 before each sampling. The SPME fiber was directly inserted in the White Cell reactor or
215 brown glass bottle for 30 min at room temperature for the collection of gas-phase N_2O.
216 The analysis was performed using a GC-MS (Agilent, USA) fused-silica capillary
217 column (HP-5MS, J & W Scientific, Folsom, CA, USA, 30 m × 0.25 mm I.D., 0.25 μm
218 film thickness). The carrier gas was high purity helium (99.999％, 1.0 mL/min). The
219 mass spectrometer was operated in the electron ionization (EI) mode at the electron
220 energy of 70 eV. Thermal desorption of retained compounds on fiber was carried out at
221 260 ℃ in splitless mode. A blank analysis was performed prior to running a sample
222 analysis.

3 Results and discussion

3.1 Effect of nitrate on surface species formed from the uptake of SO_2 onto hematite

In situ DRIFTS experiments were carried out on humid hematite, pure nitrate and a series of hematite-sodium nitrate mixtures with 2-90% of mass fractions of nitrate, respectively. Each experiment was performed at 298 K with 30 mg of sample to investigate the effects of nitrate on the uptake of gas-phase SO_2 onto the sample particle surface and the nature of the formed surface-bound species.

3.1.1 Surface sulfur-containing species

Figure 1a shows the in situ DRIFT spectra of surface species produced on pure hematite after exposure to SO_2. Four prominent peaks at 1261, 1219, 1158 and 1056 cm^{-1} and three weak shoulder peaks at 1361, 1337 and 1000 cm^{-1} are readily observed in the spectra. The intensities of these peaks increase as the reaction proceeds. These peaks can be assigned to adsorbed bisulfate and/or sulfate on the particle surface based on assignments in previous studies (Yamaguchi et al., 1986; Watanabe et al., 1994; Persson and Lovgren, 1996; Hug, 1997; Sugimoto and Wang, 1998; Nanayakkara et al., 2012). Watanabe *et al* observed infrared absorption peaks at 1360, 1270, 1150 and 1020 cm^{-1} for the sulfated hematite at 25 ℃ (Watanabe et al., 1994), and suggested that the peak at 1270 cm^{-1} was assigned to the symmetric stretching vibration mode of S=O and the peak at 1150 cm^{-1} was assigned to the asymmetric stretching vibration mode of S-O. A transmission FTIR study on SO_2 reacted TiO_2 surface has also shown peaks at 1361, 1297, 1172, 1116, 1050 and 1000 cm^{-1}, which were assigned to adsorbed sulfate species. The peak at 1335 cm^{-1} was also observed by Nanayakkara *et al*. and was thought to be most likely due to the

245 formation of sulfate (Nanayakkara et al., 2012). Therefore, in the present study, the
246 prominent peaks at 1261, 1158, 1056 and 1000 cm^{-1} reflect the formation of adsorbed
247 sulfate. Additionally, peak fitting using a combination of Lorenztian and Gaussian
248 lineshapes to deconvolute overlapping peaks of every single spectrum of an experiment
249 shows that the peaks at 1261 and 1158 cm^{-1} simultaneously increase in intensity as the
250 reaction time increases, while the peak at 1219 cm^{-1} shows a completely different
251 behavior (see Fig. S4 in the Supplement). The peak at 1219 cm^{-1} rapidly grows in the
252 early stage of the reaction, reaches a plateau, and then slightly decreases in intensity as
253 the reaction proceeds, implying that the peak at 1219 cm^{-1} should be assigned to different
254 surface species and this species undergoes secondary chemistry on the sample surface.
255 Faguy *et al* studied the structure of bisulfate and sulfate adsorbed on the Pt (111) surface
256 by potential difference Fourier transform infrared spectroscopy and found that a
257 maximum at 1227-1250 cm^{-1} was consistent with adsorbed bisulfate or adsorbed sulfate-
258 H_3O^+ ternary complexes on the Pt (111) electrode surface (Faguy and Marinković, 1996).
259 Hug (1997) found that a peak at or above 1200 cm^{-1} appeared after drying of a hematite
260 layer treated with sulfate at pH 3.6 or with hematite in contact with aqueous sulfate
261 solutions acidified to below pH 2 with HCl. He suggested that the conversion of aqueous
262 sulfate to bisulfate occurred during acidification, and thus the peak around 1200 cm^{-1} was
263 assigned to the transformation from monodentate to bidentate coordination caused by
264 drying or to the formation of bisulfate. Sugimoto and Wang (1998) further revealed that
265 the adsorption mode of sulfate changed from monodentate to bidentate with decreasing
266 pH and that the bidentate adsorption on {012} and {*1m*0} surfaces of hematite became
267 dominant at pH $\leq$ 1.0, and they suggested that the enhancement of the peak at 1205 cm^{-1}

with direct drying of a wet sample at pH 3.6, found by Hug (1997), seemed to be due to the pH drop during the drying process. The attribution of the peak at around 1200 cm^{-1} remains controversial, however, the appearance of this peak undoubtedly reflects the enhancement of surface acidity. Therefore, in the present study, the increase in the peak intensity at 1219 cm^{-1} with the increase of reaction time indicates the increased surface acidity (Yamaguchi et al., 1986; Persson and Lovgren, 1996; Faguy and Marinković, 1996; Hug, 1997). The slight decrease in intensity of the peak at 1219 cm^{-1} after it reaches the maximum may be due to partial dissolution of hematite along with consumption of surface acidic species, which would lead to the formation of Fe^{3+} ions and some other surface species on the water-containing surface (Chun and Quon, 1973; Shi et al., 2011).

Figure 1b shows typical spectra of the oxidation of SO_2 on FN-24 recorded as a function of time in the range of 1500 to 900 cm^{-1}. A prominent peak at 1158 cm^{-1}, a shoulder peak at 1190 cm^{-1} and two weak peaks at 1080 and 987 cm^{-1} are observed in the spectra. These peaks can be assigned to surface-coordinated sulfate species, that is, bidentate surface sulfate complex (Zhang et al., 2006; Persson and Lovgren, 1996; Hug, 1997; Peak et al., 1999). Additionally, it is also possible that the feature at 1190 cm^{-1} is assigned to bisulfate (HSO_4^-) or sodium sulfate ($NaSO_4^-$) sorbed as a monodentate complex on the iron oxide surface, or monodentate sulfate that is hydrogen bonded to an adjacent surface site (Hug, 1997; Peak et al., 1999). In addition, Fe^{3+} ions is present due to the partial dissolution of hematite in the water-containing acidic surface during the reaction (Chun and Quon, 1973; Shi et al., 2011), and an iron (III) bisulfate complex (Fe–HSO_4^{2+}) can also potentially explain the observed feature at 1190 cm^{-1} (Peak et al., 1999).

These results indicated that SO_2 can also be oxidized to sulfate on the surface of the hematite-nitrate mixture. The spectrum lineshapes are different from those of hematite, and the most apparent FTIR feature corresponding to the increase of surface product on FN-24 is the rapidly growing peak at 1158 cm^{-1}, indicating that the adsorbed sulfate is the dominant oxidation product. Therefore, NO_3^- ions in the nitrate-hematite mixture promote the heterogeneous uptake of SO_2 and impact the formation of surface species and the adsorption mode of the formed surface species. A spectral peak-fitting program using mixed Gaussian-Lorentzian peak fitting is employed to fit peaks to the last spectrum in Fig. 1b. As shown in Fig. 2, the region from 1400 to 900 cm^{-1} is composed of three major peaks at 1207, 1155 and 1094 cm^{-1}, respectively. A very weak peak at 986 cm^{-1} cannot even be seen in Fig. 2. The relative intensity of the observed peaks at 1207, 1155, 1094 and 986 cm^{-1} is approximately 5.6:16.1:2.2:0.1, respectively. The presence of the peak at 1207 cm^{-1} indicates that the FN-24 surface after the experiment is still acidic. Moreover, compared with that of the hematite-only substrate (see Section S6 in the Supplement), weak absorption peaks at 1080, 1050 and 966 cm^{-1} appear in the initial stage of heterogeneous conversion of SO_2 and then gradually disappear or are not easily observed with increased exposure time. These peaks should be assigned to the stretching motion of adsorbed sulfite and/or bisulfite (Zhang et al., 2006). The changes in intensity of these weak absorption peaks implies that the formation of SO_3^{2-} and/or HSO_3^- and their subsequently rapid consumption on the particle surface. The rapidly growing peak at 1158 cm^{-1} as the reaction proceeds also suggests that SO_3^{2-} and HSO_3^- are further oxidized in the presence of nitrate and less SO_3^{2-} and HSO_3^- are left when compared with that of hematite-only substrate.

3.1.2 Surface nitrogen-containing species

It should be noted that, compared to the peaks of the formed surface-adsorbed sulfate, some very low intensity signals appear in the region of 3800 to 1350 cm^{-1} during the same experiment with FN-24 (also see Fig. S5 in the Supplement). Figure 3 shows DRIFTS spectra following SO_2 uptake on FN-24 particles as a function of reaction time in this region. Negative peaks at 1599, 1587 and 1567 cm^{-1} decrease in intensity with increased exposure time. These peaks are assigned to bridging, bidentate and monodentate nitrate, respectively (Hixson et al., 2011; Underwood et al., 1999). This indicates the loss of adsorbed nitrate on FN-24 and suggests that nitrate not only participates in the heterogeneous conversion of SO_2 on FN-24 but also have been consumed during the reaction. This result is consistent with the formation of nitrogen-containing species such as N_2O and HONO (discussed later in Sect. 3.4). However, it should be pointed out that the amount of the decay of nitrate is small during the reaction, which also results in small amounts of N_2O and HONO.

Several weak peaks in the 1535-1440 cm^{-1} region grow with increasing exposure time. These peaks can be assigned to adsorbed nitrite. The peaks at 1506 and 1487 cm^{-1} are assigned to the υ_3 mode of bridging nitro-nitrito NO_2^- and the υ_3 mode of bridging monodentate nitrito NO_2^- respectively, suggesting the formation of very small amounts of nitrite (Hixson et al., 2011).

Molecularly adsorbed nitric acid and different nitric acid-water complexes, characterized by the peaks at 1716, 1697, 1686 and 1676 cm^{-1} (McCurdy et al., 2002; Ramazan et al., 2006; Finlayson-Pitts et al., 2003), are also observed. These peaks are

ascribed to the υ_2 mode of the asymmetric NO_2 stretch in nitric acid (monomer or when complexed to water or another HNO_3) (McCurdy et al., 2002; Ramazan et al., 2006; Finlayson-Pitts et al., 2003), and the peaks at 1716, 1697, 1686 and 1676 cm^{-1} are due to $HNO_3 (H_2O)_n$, $HNO_3 H_2O$, $(HNO_3)_2$ and $HNO_3 (H_2O)_2$ on the surface, respectively. These peaks increase in intensity with increased exposure time. This result confirms that adsorbed HNO_3 is formed from the combination of surface H^+ with NO_3^- as the reaction proceeds. The formation of HNO_3-H_2O complexes indicates that nitric acid is stabilized by water on the particle surface (McCurdy et al., 2002; Ramazan et al., 2006; Finlayson-Pitts et al., 2003). As a result, no gas phase HNO_3 was observed in White cell-FTIR experiments as discussed later. Compared to the assignments of molecularly adsorbed nitric acid, molecular nitric acid complexed to water and complexed to HNO_3 itself in previous reports, these peaks have blue shifted by about 6 cm^{-1} (McCurdy et al., 2002; Ramazan et al., 2006), indicating that the asymmetric NO_2 stretch in nitric acid may be affected by some other interaction, and the interaction may result in the distortion of the molecular symmetry of these complexes (Peak et al., 1999).

Two weak shoulder peaks at 1746 and 1732 cm^{-1} are seen to grow as the surface is exposed to SO_2. These two peaks should be attributed to the asymmetric $\upsilon_a(NO_2)$ stretch of N_2O_4 adsorbed on the surface, indicating the formation of adsorbed N_2O_4 (Goodman et al., 1999; Finlayson-Pitts et al., 2003). These peaks overlap with those of adsorbed HNO_3 and increase in intensity with the amount of adsorbed nitric acid on the surface. As previously reported, N_2O_4 can interact with HNO_3 and/or HNO_3-H_2O water complexes on particle surface through hydrogen bonds, in addition to the interactions with H_2O (Finlayson-Pitts et al., 2003). This further indicates that the formed N_2O_4 may be held on

particle surface with nitric acid and H_2O present. This is consistent with the fact that no gas phase N_2O_4 was detected in White cell-FTIR experiments as discussed later. Surface N_2O_4, which can oxidize many organic and inorganic compounds, was observed as the crucial oxidant for the oxidation of surface sulfite (Liu et al., 2012). Therefore, the presence of a very small amount of N_2O_4 on particle surface may contribute to the oxidation of surface sulfite and the formation of sulfate and adsorbed nitrite.

3.1.3 Surface hydroxyl groups

Two negative absorption peaks are observed at 3661 and 3631 cm^{-1} and grow in intensity as the reaction proceeds. These negative peaks have been previously reported and attributed to the loss of OH groups from the surface. The peaks at 3661 and 3631 cm^{-1} are stretching vibration modes of isolated surface hydroxyl groups bonded to the surface iron ions of octahedral sites and tetrahedral sites, respectively (Watanabe et al., 1994), which implies that surface OH groups are involved in the reaction and are reaction active sites for SO_2 (Goodman et al., 2001). Pure hematite shows similar absorption. Another weak broad absorption peak extending from 3500 to 2520 cm^{-1} slowly increases in intensity with the increase of reaction time. This broad peak is primarily associated with O-H vibration of hydrogen-bonded OH groups of acid and should be assigned to molecular nitric acid complexed to water or to some extent complexed to HNO_3 itself (Börensen et al., 2000; Goodman, et al., 1999; Ramazan et al., 2006; Finlayson-Pitts et al., 2003), which is consistent with the formation of surface-adsorbed HNO_3 discussed earlier.

Overall, the results indicate that nitrate participates in the heterogeneous reactions of SO_2, changes the conversion pathway of SO_2 and the formation rate of sulfate, and leads

to the formation of surface HNO_3, N_2O_4 and NO_2^- species. A summary of the assignments for the surface species peaks observed in this study based on frequencies reported in earlier studies is given in Table 1.

3.2 Effect of nitrate on the rate of sulfate formation and uptake coefficient for SO_2 on hematite-nitrate mixture at 298 K

The formation rates of sulfate on different samples were investigated. All of the DRIFTS experiments were performed at 298 K with 30 mg of sample, and the amount of sulfate on each sample after DRIFTS experiment was determined by ion chromatography to quantify the sulfate formation rate $d[SO_4^{2-}]/dt$. It is found that over a large concentration range the integrated sulfate absorption (1000 cm^{-1} to 1400 cm^{-1}) is proportional to the sulfate concentration. The formation rate is therefore translated from the integrated sulfate absorbance of the spectrum to the total number of sulfate ions on the sample after the reaction by a conversion factor. The conversion factor is obtained from a calibration plot with integrated sulfate absorption vs. number of sulfate ions formed at the end of an experiment, and a value of $f = 2.58 \times 10^{18}$ (ions g^{-1} integrated absorption $units^{-1}$) is calculated. Since the absorption peaks of different reaction product species overlap one another, the peaks were deconvoluted before integration in some experiments.

The gas-phase concentrations of the reactive gases in a continuous flow were kept constant during the DRIFTS experiments and since O_2 was in great excess compared to SO_2, the concentration of O_2 could be regarded as constant. The number of sulfate ions formed at the initial stage of reaction is generally considered to be small relative to the number of reactive surface sites, and thus the latter at initial stage can be assumed to be

constant (Börensen, et al., 2000). Therefore, the reaction order can be determined from a bilogarithmic plot of initial rate of sulfate formation (log(d[SO_4^{2-}]/dt)) vs. the concentration of SO_2 (log[SO_2]), as previously reported (Börensen et al., 2000; Wu et al., 2011). For this purpose, the experiments with different SO_2 concentrations were performed, and the sulfate formation rate d[SO_4^{2-}]/dt was obtained from the slope of the initial linear portion (0-60 min) in the curve of sulfate formation as a function of time. No saturation effects on sulfate formation were observed. For the mixture such as FN-24 used in this study, the plot gave a slope of 1.09 ± 0.10 (2σ), which indicates a reaction order of 1 for SO_2. The reaction order with respect to SO_2 was also examined from White cell-FTIR experimental data by examining the rates of SO_2 decay. The calculated result is consistent with that using DRIFTS data (correlation coefficient of $\ln[SO_2]_0/[SO_2]$ vs. time (t) was greater than 0.99). That is, the heterogeneous oxidation of SO_2 on the hematite-nitrate mixture was still a pseudo-first-order reaction.

The reactive uptake coefficient (γ) is defined as the rate of sulfate formation on the surface (d[SO_4^{2-}]/dt) divided by the total number of surface collisions per unit time (Z).

$$\gamma = \frac{d[SO_4^{2-}]/dt}{Z} \quad (1)$$

$$Z = \frac{1}{4} \times A_s \times [SO_2] \times \nu \quad (2)$$

$$\nu = \sqrt{8RT/\pi M_{SO_2}} \quad (3)$$

where ν is the mean molecular velocity of SO_2, A_s is the effective sample surface, R is the gas constant, T is the temperature and M_{SO2} is the molecular weight of SO_2 (Ullerstam,

et al., 2003). Two extreme cases of effective sample surface are usually considered for calculating the uptake coefficient (Ullerstam et al., 2002). If the reaction probability is high, the reactants would have no time to diffuse into the sample before reacting and the effective surface area will be the geometric surface area of the sample holder ($A_{geometric}$). If the reaction probability is low, the reactants may have enough time to diffuse into the entire sample and thus the BET surface area (A_{BET}) would more appropriately represent the effective area. Therefore, upper and lower limits of uptake coefficients can be calculated using the geometric and BET surface area as the reactive surface area, respectively (denoted as $\gamma_{geometric}$ and γ_{BET}, respectively).

Table 2 shows the sulfate formation rates and the two kinds of uptake coefficients of SO_2 on hematite and the hematite-nitrate mixtures at 298 K. The sulfate formation rate and the two kinds of uptake coefficients first increase and then decrease with increasing mass fraction of nitrate, and no sulfate formation is observed on pure sodium nitrate. For mixtures, the FN-24 sample presents the highest sulfate formation rate. Correspondingly, the FN-24 sample shows the highest $\gamma_{geometric}$, and its $\gamma_{geometric}$ is about 5.5 times higher than that of hematite alone. Although the sulfate formation rate for FN-24 is higher than that for FN-48, the BET uptake coefficient γ_{BET} for FN-24 is less than that for FN-48. This is mainly because that the FN-48 has smaller BET surface area than the FN-24, and hence the FN-48 presents the highest γ_{BET}. Its γ_{BET} is about 8 times higher than that of pure hematite. Therefore, the reaction behavior of SO_2 adsorbed on hematite is altered by the availability of nitrate. An appropriate amount of nitrate greatly enhances the reactivity of the hematite-nitrate mixtures and favors the formation of sulfate on hematite. The promotion effect of a low to moderate amount of nitrate should receive close attention

because the nitrate content is close to that in ambient particles (Ho et al., 2003), and this effect may help to predict the formation of sulfate aerosols in the atmosphere.

3.3 Effect of nitrate on heterogeneous reactivity of SO_2 on hematite at 298 K

The White cell-FTIR can be used to trace gaseous reactants and possible gaseous products formed from the heterogeneous reaction of SO_2, but it cannot be used to observe surface species formed on the sample surface. In situ White cell-FTIR spectra collected from exposure of the FN-24 sample to 50 ppm of SO_2 at room temperature are shown in Fig. 4. The strong absorption peaks at 1373, 1360, and 1348 cm^{-1} and the weak ones at 1163 and 1135 cm^{-1} are readily observed in the spectra. These peaks are assigned to the characteristic peaks of gaseous SO_2 (Fu et al., 2007; Zhang et al., 2006). The intensities of these peaks in the spectra decrease rapidly as the reaction proceeds, indicating that the concentration of SO_2 decreases while it reacts on the surface of FN-24. The other FN series and pure hematite samples upon exposure to 50 ppm of SO_2 at room temperature show similar absorption but different rates of SO_2 consumption, revealing that the sample reactivity varies with mass fractions of sodium nitrate. No uptake of SO_2 is observed on the pure sodium nitrate. The results indicate that the reactivity increases first and then decreases with increasing mass fraction of sodium nitrate in the samples. This is consistent with that observed in DRIFTS experiments.

3.4 Effect of nitrate on gas-phase products from the heterogeneous uptake of SO_2 on hematite

It is worth noting that several absorption peaks of gaseous HONO appear in the spectra in the White cell-FTIR experiment by exposing the FN series samples to lower

concentrations of SO_2. Although adsorbed HNO_3 has been detected during the DRIFTS experiments, gas phase nitric acid has not been observed in White cell-FTIR experiments, suggesting that molecular nitric acid is firmly adsorbed on the particle surface in the presence of water. Figure 5 shows the representative in situ FTIR spectra collected from exposure of the FN-90 sample to 12.5 ppm of SO_2 for different times. A difference spectrum shown in Fig. 5e was obtained by subtracting the spectrum in Fig. 5c from that in Fig. 5d. As shown in Fig. 5, there are no absorption peaks of gas-phase HONO before 430 min but several weak HONO absorption peaks centered at 1262, 850 and 790 cm^{-1} are observed when the reaction time is prolonged to 1170 min (Fig. 5d) (Wingen et al., 2000). The difference spectrum shown in Fig. 5e further confirms the existence of HONO, revealing that a trace amount of gaseous HONO is formed during the reaction of SO_2 on the hematite-nitrate mixture. To the best of our knowledge, this is the first observation of the formation of HONO in such a nitrate-containing reaction system. Observation of HONO formation is of particular significance because it plays an important role in the degradation of primary and secondary atmospheric pollutants by serving as a major source of hydroxyl radicals. HONO formed from heterogeneous reaction of nitrogen dioxide has been extensively studied on different materials like mineral dust particles and soot (Finlayson-Pitts et al., 2003; Arens et al., 2001), and HONO is known to be in equilibrium with NO and NO_2 in the gas phase via its self-reaction (Pitts et al., 1984). However, the heterogeneous reaction of nitrogen dioxide and the self-reaction of HONO may be negligible in our system because no absorption peaks of gas-phase NO and NO_2 in the spectral range from 1200 to 1900 cm^{-1} are observed. It is possible that gaseous NO and NO_2 are present at concentrations below detection limits. But on the other hand, the

weak absorption peaks of HONO may suggest the very low HONO partial pressure, and hence the self-reaction of HONO is probably not relevant at such a low HONO pressure.

The result also suggests that the initial surface-formed HONO may be simultaneously consumed by some secondary reactions in this system. On the one hand, no absorption peaks of HONO by exposing the FN series samples to 50 ppm SO_2 for the same reaction time were observed. This fact suggests that the possible consumption reactions of HONO may be the ones between HONO and the surface abundant reduced S(IV) species, such as sorbed or surface-coordinated H_2SO_3, HSO_3^- and SO_3^{2-} species, which led to gaseous HONO levels below detection limits before the complete consumption of these species. On the other hand, the high concentration of SO_2 means that there are much more reduced S(IV) species existing on the sample surface than those formed from the low concentration of SO_2. This also implies that HONO will be observed within a long reaction time if the high concentration of SO_2 is used. An earlier study of Martin *et al.* observed that S(IV) species can be rapidly oxidized to sulfate by HONO in acidic aqueous aerosols (Martin et al., 1981), which would support the secondary reactions of HONO with S(IV) species in our experiments and reveal the potential role of HONO in the heterogeneous conversion of SO_2. In addition, the absorption peaks between 1400 and 1800 cm^{-1} are mainly attributed to H_2O molecule vibrations. These absorption peaks gradually grow in intensity with the increase of reaction time because H_2O molecules can evaporate slowly from the humid surface of FN samples placed in the White cell.

Rivera-Figueroa et al. found that the reaction between HNO_3 and SO_2 on silica surfaces in the presence of water films does not occur (Rivera-Figueroa et al., 2003). Martin and co-workers also reported that nitric acid in solution does not react with

514 dissolved SO_2 (Martin et al., 1981). Furthermore, in our study the experiments in which
515 humid pure nitrate was exposed to SO_2 using White cell-FTIR and DRIFTS techniques
516 also show no detectable gas phase products, indicating that pure nitrate cannot interact
517 with SO_2. Therefore, considering the species in the reaction systems mentioned above,
518 these previous studies indicate that the reactions between HNO_3 and S(IV) species cannot
519 occur. Moreover, reductive dissolution of Fe (Ⅲ) oxides and reduction of Fe (Ⅲ) by
520 sulfite have been suggested as possible sources of Fe (Ⅱ) (Behra and Sigg, 1990), and
521 the formation of Fe^{2+} via heterogeneous reaction of SO_2 oxidation on the surface of Fe_2O_3
522 has already been verified by measuring the amount of Fe^{2+} during the reaction (Zhang et
523 al., 2007; Ansari et al., 1997). Therefore, among the possible surface species in our
524 reaction system, Fe^{2+} is the only reduced species that can react with NO_3^- in the presence
525 of H^+. In other words, the only formation pathway of HONO is the reduction of NO_3^- by
526 the reductive Fe^{2+} in the presence of H^+, while the reductant Fe^{2+} can be fed from the
527 recycle from the reduction of Fe^{3+} by dissolved SO_2. HONO formation processes in the
528 atmosphere are still under discussion, especially during daytime where large
529 discrepancies are found between mixing ratios calculated from known gas phase
530 chemistry and measured daytime mixing ratios (Kleffmann et al., 2005). Our results also
531 suggest that the heterogeneous reaction of SO_2 on nitrate-containing hematite may serve
532 as a potential source for HONO, which may have implications on the oxidant chemistry
533 in the atmosphere. However, the low yield of gaseous HONO may suggest that the
534 contribution of HONO by this pathway to the atmospheric gas phase HONO may be
535 negligible, but the formation of unreleased HONO in the particles may be significant for
536 the conversion of SO_2 and the formation of sulfate in the atmosphere.

In addition, it is interesting to note that N_2O is formed in the process of the heterogeneous uptake of SO_2 on the hematite-nitrate mixtures at both low and high SO_2 concentrations. As shown in Fig. 5, two N_2O absorption peaks at 2235 and 2208 cm^{-1} appear and slowly grow in intensity with the increase of reaction time (Hussain and Rahman, 2006), indicating that gas-phase N_2O is produced in the FT-IR experiments. The concentration of N_2O gradually increases and approaches a constant (ca. 418 ppb) as the reaction proceeds (see Fig. 5f). The gas-phase concentrations of N_2O are determined according to a linear relationship between the integrated area of the gaseous N_2O absorption peaks in the range 2258-2160 cm^{-1} and its concentration (r^2 = 0.996). The linear relationship is obtained using in situ White cell-FTIR and different concentrations of N_2O standard gas. The observed formation of N_2O is of particular importance because it is an extremely influential greenhouse gas and directly involved in global warming as well as in the destruction of ozone in the stratosphere. It has been reported that sulfur (IV) species such as H_2SO_3 can be easily oxidized by HONO at low pH (0.6-3.2) and the gas phase product is N_2O (Martin et al., 1981). Therefore, it is reasonable to speculate that N_2O is formed from the reduction of HONO by S(IV) species such as sorbed or surface-coordinated H_2SO_3, HSO_3^- and SO_3^{2-} species on the mixture sample surface before HONO is released (Pires et al., 1996; Pires et al., 1997). This observation provides evidence for the formation of nitrous oxide from the hematite-nitrate mixtures at ambient temperature, and suggests a new potential atmospheric source of N_2O. This source is currently not accounted for in the global N_2O budget. The result may help to explain why the sources of N_2O exceed the estimated sinks in the atmosphere and the observed increase in atmospheric N_2O. However, it should be pointed out that the high surface to

volume ratio of the experiments may lead to relatively more N_2O than in the atmosphere. Meanwhile the lifetime of HONO in the atmosphere is probably limited by photolysis. The relative importance of this source needs further study.

To further confirm the formation of HONO and N_2O, we also performed heterogeneous reactions of SO_2 (50 ppm) on humid hematite, FN-24 and FN-90 in the presence of O_2 (21% v/v) in three brown glass bottles in the dark for 3-7 days. The dark condition is selected to avoid the photolysis of HONO and the photochemistry of adsorbed nitrate (Schuttlefield et al., 2008). The selected long reaction time favors the release of the produced HONO and the accumulation of N_2O. Figure 6 shows the digital photos of the three samples after reaction with SO_2 in the dark at room temperature for about 7 days. Interestingly, the heterogeneous reactions of SO_2 on the surfaces of FN-24 and FN-90 present unique phenomena, and some liquid drops cover the interior walls of glass bottles, which is different from that presented by the reaction of SO_2 on the pure hematite. The latter does not show the similar phenomenon. The liquid drops show strong acidity which has been measured with pH test paper (the pH was about 1). Ion chromatography analysis shows that the liquid drops mainly contain sulfate ions while the concentration of nitrate ion is below the detection limit. These results indicate that the liquid drop is sulfuric acid. The appearance of the liquid drops should be attributed to the presence of gas phase HONO. Gas phase HONO transforms SO_2 that is present in the gas-phase or adsorbed on the bottle walls into sulfuric acid, while reactive HONO is produced from the heterogeneous reaction of SO_2 on the surface of the hematite-nitrate mixture and the subsequent release. The HONO vapor adsorbs onto the interior wall of the glass bottle, and together with H_2O initiates the oxidation of SO_2 and the subsequent formation of

H_2SO_4. Additionally, the gas-phase species in the three glass bottles were analyzed by using SPMS/GC-MS technique, and N_2O is only found from the reactions of SO_2 on FN-24 and FN-90, no NO, NO_2 and N_2O_4 are detected (see Fig. S6 in the Supplement). Therefore, considering the experimental results mentioned above, the formation of HONO and N_2O during the reaction of SO_2 on the hematite-nitrate mixture has been further verified by this experiment, which is consistent with the observations from in situ White Cell-FTIR experiments. This experiment also verifies that N_2O and HONO can be produced from the reaction of SO_2 on the hematite-sodium nitrate mixtures not only in daytime but also at night. Although the concentration of the formed HONO cannot be accurately measured during the process of the heterogeneous uptake of SO_2 on the hematite-nitrate mixture because the formed HONO is being continuously consumed on the particle surface, it may be important not only in daytime but also at night for the conversion of atmospheric SO_2 and the formation of atmospheric sulfate. Such aspects should be further explored in future studies.

3.5 Effect of nitrate on the morphology of surface product formed from the uptake of SO_2 onto hematite

Scanning electron micrographs of sample particles before and after reaction with gaseous SO_2 were obtained from a Philips XL-30 scanning electron microscope equipped with an energy dispersive X-ray spectrometer (SEM-EDX). Figure 7 shows SEM images of FN-24 and FN-90 particles before (Fig. 7a and c) and after (Fig. 7b and d) exposure to gaseous SO_2 in the DRIFTS experiments. The two unreacted samples show the morphology of aggregated particles and consist of primary particles with an averaged particle size of over 100 nm. After the reaction with SO_2, there are some flaky substances

606 covering some particle surfaces. EDX analysis shows that the flaky substance is
607 composed of 57.89% O, 11.70% Na, 11.48% S and 18.93% Fe (Fig. 7e). The
608 characteristic peaks in the EDX spectrum indicates that no nitrogen is detected on the
609 flaky substance, indicating the formation of sulfate on the particle surface and the change
610 in particle morphology. This result should be attributed to the enhanced formation of
611 sulfate on the hematite surface due to the presence of nitrate. It should be noted that we
612 cannot observe a similar phenomenon on the pure hematite after exposure to SO_2.

613 **3.6 Role of surface adsorbed water under the influence of nitrate**

614 Previous studies indicate that surface-adsorbed water plays an important role in the
615 heterogeneous chemistry of atmospheric SO_2 (Nanayakkara et al., 2012). However, little
616 is known about the role of surface-adsorbed water in the heterogeneous oxidation of SO_2
617 on hematite-nitrate mixture. Therefore, the role of surface-adsorbed water in the
618 heterogeneous oxidation of SO_2 on FN-24 was further investigated using in situ DRIFTS.
619 In order to prevent the sample particles from being brought out from the in situ chamber,
620 a vacuum wasn't applied during these experiments. The sample was first pretreated at
621 preset temperature for 60 min in a stream of Ar in a total flow of 100 mL min^{-1}. The
622 preset temperatures were 298, 303, 373, 423, 473 and 573 K, respectively. After 60 min
623 the heated sample in the reaction chamber was cooled to 298 K under Ar flow, and a
624 background spectrum of the unreacted powder sample was collected. Subsequently, IR
625 spectra were collected as a function of reaction time after being exposed to gaseous
626 reactants. The results are shown in Fig. 8. The pre-treated sample at 373, 423 and 473 K
627 enhances the reactivity of hematite, and the sulfate formation rates at 373 and 423 K
628 increase by a factor of 1.28 and 1.25 compared with that at 298 K, respectively,

indicating that the presence of appropriate amount of water on particle surface will favor the heterogeneous conversion of SO_2. However, with a further increase in pre-treated temperature the reactivity decreases, and the sample pre-treated at 573 K shows even lower reactivity than that at 298 K. Pre-treatment of the sample is known to mainly remove surface- adsorbed water, and, at higher temperature, surface dehydration occurs. The observed increases in the reactivity of the sample pre-treated at 373 and 423 K are due to the partly removal of physiadsorbed water, which may serve as an inhibitor for the SO_2 oxidation by blocking access to the active sites. Samples pre-treated at higher temperatures (573 K) displays removal of the physiadsorbed water along with partly desorption of surface hydroxyl groups (EgashIra et al., 1981), resulting in a decrease in the sample reactivity. In agreement with other studies, surface hydroxyl groups can be the active sites for the conversion of SO_2.

3.7 Proposed mechanism of SO_2 uptake on hematite-nitrate mixtures

On the basis of the experimental observations described above, a reaction mechanism for the heterogeneous reaction of SO_2 on the hematite-nitrate mixture is proposed. Previous studies have shown that nitrate ions can be readily solvated by adsorbed water molecules under ambient conditions due to their hygroscopic nature (Hoffman et al., 2004), and thus nitrate in mixture sample will make more water molecules be adsorbed on the particles when the prepared mixture sample is kept in a desiccator at 68% RH for 48 h, and leads to weak water loss during the purge and subsequent reaction processes. The adsorbed water will favor the uptake of SO_2 and the formation of S(IV) species (Zhang et al., 2007; Preszler Prince et al., 2007). Therefore, in the initial stage of heterogeneous conversion of

651 SO_2 on the nitrate-hematite mixture, the following reactions will occur (Zhang et al.,
652 2007):

653 $SO_2 + H_2O \rightarrow H_2SO_3$ (R1)

654 $H_2SO_3 \rightarrow H^+ + HSO_3^-$ (R2)

655 Earlier studies of SO_2 adsorption on metal oxides have shown that Lewis acid sites,
656 hydroxyl groups and oxygen vacancies can all play a role in the surface chemistry
657 (Goodman et al., 2001; Fu et al., 2007; Baltrusaitis et al., 2007, 2010). Surface hydroxyl
658 groups are involved in the adsorption of sulfur dioxide, and in particularly, sulfur dioxide
659 reacts with either one surface O–H group to yield adsorbed bisulfite or two surface O–H
660 groups to yield adsorbed sulfite and water. In the current study, the used nitrate-hematite
661 mixtures are still loose fine powders after they are saturated at 68% RH for 48 h, and
662 there may be several water molecule layers resisting on humid sample surfaces. Therefore,
663 surface sulfate and/or bisulfate can also be produced on the nitrate-hematite mixture
664 particles through surface active oxygen and hydroxyl, while the active oxygen and
665 hydroxyl can be formed from the interaction of O_2 and H_2O with the surface of hematite
666 (Baltrusaitis et al., 2007). The formation mechanism of the surface sulfate and/or
667 bisulfate during initial reaction stages should also be the same as that reported previously
668 (Goodman et al., 2001; Baltrusaitis et al., 2007; Fu et al., 2007; Zhang et al., 2007). That
669 is, the gaseous SO_2 reacts with surface active oxygen and hydroxyl to form surface S(IV)
670 species (i.e. adsorbed sulfur species and surface-coordinated HSO_3^- and SO_3^{2-}), and then
671 these S(IV) species are further oxidized to surface S (VI) species including SO_4^{2-} and/or

672 HSO_4^- in the presence of O_2 and H_2O (Fu et al., 2007; Zhang et al., 2007; Preszler Prince
673 et al., 2007).

674 The reactions mentioned above will lead to the formation of an acidic surface. On the
675 acidic surface, hematite will be partially dissolved to give Fe^{3+} ions in the water-rich
676 surface (Chun and Quon, 1973; Shi et al., 2011), which in turn oxidizes HSO_3^- to form
677 SO_4^{2-}. As previously reported, Fe^{2+} ions are generated during this process (Behra and
678 Sigg, 1990; Ansari et al., 1997; Zhang et al., 2007).

679 $$6H^+ + Fe_2O_3 \rightarrow 2Fe^{3+} + 3H_2O \quad \text{(R3)}$$

680 $$2Fe^{3+} + HSO_3^- + H_2O \rightarrow 2Fe^{2+} + SO_4^{2-} + 3H^+ \quad \text{(R4)}$$

681 It is well established that the nitrate ion is a strong oxidizing agent in highly acidic
682 solutions that is capable of changing the oxidation state of reduced species (Burley and
683 Johnston, 1992). As the above reactions proceed, the surface of the mixed hematite-
684 nitrate sample becomes more acidic, and adsorbed nitric acid and nitric acid-water
685 complexes are gradually formed on the surface. Once the surface becomes sufficiently
686 acidified, the interaction between nitric acid and Fe^{2+} ion occurs on acidic surface, and
687 the Fe^{2+} ion is oxidized and HONO is produced (Summers, 2005), as given in the
688 following ionic equation:

689 $$2Fe^{2+} + 3H^+ + NO_3^- \rightarrow 2Fe^{3+} + HONO + H_2O \quad \text{(R5)}$$

690 The re-generated Fe^{3+} further oxidizes the S(IV) species to S(VI) species and produces
691 Fe^{2+} ions. With the cycle of the above reactions, more and more sulfates and HONO are
692 produced. As shown in previous studies, S(IV) species can be rapidly oxidized to sulfate

693 by HONO, and HONO can be reduced to N_2O in acidic aqueous aerosols (Martin et al.,
694 1981; Pires et al., 1996, 1997). Thus, the formed HONO is also considered to react
695 promptly with surface S(IV) species (i.e. sorbed H_2SO_3, HSO_3^- and SO_3^{2-}) before it
696 escapes to the gas phase, which also results in the formation of N_2O and more sulfates on
697 the particle surface. As reported previously (Martin et al., 1981), the stoichiometry should
698 be as follows:

699 $2HONO + 2H_2SO_3 \rightarrow 2H_2SO_4 + N_2O + H_2O$ (R6)

700 $2HONO + 2HSO_3^- \rightarrow 2SO_4^{2-} + N_2O + H_2O + 2H^+$ (R7)

701 $2HONO + 2SO_3^{2-} \rightarrow 2SO_4^{2-} + N_2O + H_2O$ (R8)

702 An alternate mechanism involving consumption of HONO and formation of sulfate is
703 based on that proposed by Finlayson-Pitts et al. (2003) and Liu et al. (2012). That is,
704 reaction of the surface formed HONO with HNO_3 on the surface generates $NO^+NO_3^-$.
705 This reaction can be thought of as a reaction of NO_3^- with NO^+ formed from the reaction
706 of HONO with the HNO_3, i.e., the reverse of the overall NO_2 hydrolysis reaction. The
707 reaction process may be as follows:

708 $HONO_{(surface)} + HNO_{3\,(surface)} \rightarrow NO^+NO_3^-{}_{(surface)} + H_2O$ (R9)

709 Some $NO^+NO_3^-{}_{(surface)}$ isomerizes to surface asymmetric $ONONO_2$, and then $ONONO_2$
710 converts to small amount of N_2O_4 (Finlayson-Pitts et al., 2003; Liu et al., 2012). The
711 formed N_2O_4 interacts strongly with water and adsorbed HNO_3 and would be more likely
712 present on the surface (Finlayson-Pitts et al., 2003). Some $NO^+NO_3^-{}_{(surface)}$ oxidizes
713 surface S(IV) species to sulfate, while $NO^+NO_3^-$ itself is reduced to nitrite (M represents

the surface metal sites). This can explain small amounts of N_2O_4 and nitrite observed in our study:

$$NO^+NO_3^-{}_{(surface)} \rightarrow ONONO_{2\ (surface)} \rightarrow N_2O_{4\ (surface)} \quad \text{(R10)}$$

$$NO^+NO_3^-{}_{(surface)} + MSO_3 \rightarrow MSO_4 + NO^+NO_2^- \quad \text{(R11)}$$

Once the surface S(IV) species have been completely consumed, the remaining $NO^+NO_3^-$ will react with surface adsorbed water to generate HONO and adsorbed HNO_3 (Finlayson-Pitts et al., 2003), and subsequently the formed HONO through the reaction of $NO^+NO_3^-$ with water and the unconsumed HONO by S(IV) species will be slowly released into the gas phase. Accordingly, HONO rather than N_2O_4 is responsible for the formation of H_2SO_4 liquid drops on the interior wall of the glass bottle in the dark.

$$NO^+NO_3^-{}_{(surface)} + H_2O_{\ (surface)} \rightarrow HONO_{\ (g,\ surface)} + HNO_{3\ (surface)} \quad \text{(R12)}$$

Therefore, the appearance of HONO will favor the oxidation of S(IV) species on the surface and lead to the formation of more sulfates (Martin et al., 1981). With the cycle of the above reactions, more and more sulfates and N_2O are produced. Once the reduced S(IV) species on the surface have been completely consumed, the remaining and subsequently formed HONO will slowly escape into the gas phase, and be detected by FTIR.

In addition, it is well-known that N_2O can be formed during heterogeneous hydrolysis of gas-phase NO_2 via HONO on acidic oxide surfaces (Finlayson-Pitts et al., 2003; Wiesen et al., 1995). Therefore, another possibility for the formation of N_2O is similar to

the conversion proposed by Finlayson-Pitts *et al* and Wiesen *et al* (Finlayson-Pitts et al., 2003; Wiesen et al., 1995). That is, reaction of HONO and its protonated forms (H_2ONO^+ or possibly NO^+) generates hyponitrous acid, HON=NOH. The self-reaction of $(HON)_2$ then decomposes to N_2O under acidic conditions. Similar chemistry has also been proposed for the formation of N_2O under acidic conditions in the presence of SO_2 (Pires et al., 1997).

Above all, the consumed nitrate during the reaction will favor the uptake of more SO_2 molecules and produce more surface sulfate, while secondary chemistry of intermediate HONO will also result in the formation of gas phase N_2O. Furthermore, more adsorbed or surface-coordinated S(IV) species produced from higher concentrations of SO_2 also indicate that it will take a longer reaction time to observe the formation of gaseous HONO. The proposed mechanism provides new insights into some unsolved atmospheric problems such as unknown sources of N_2O and potential HONO, unknown SO_2 sinks and unknown sulfate formation pathways in the troposphere, and this chemistry also helps to explain the discrepancy between model-predicted sulfate and field observations of sulfate in the atmosphere (Laskin et al., 2003). The reaction mechanism of the heterogeneous oxidation of SO_2 on hematite in the presence of nitrate is summarized in Fig. 9.

4 Conclusions

The effects of nitrate on heterogeneous conversion of SO_2 on hematite at room temperature have been investigated. It is found that nitrate participates in the heterogeneous reactions of SO_2, changes the conversion pathway of SO_2, and leads to the

formation of HNO_3, N_2O, HONO and more sulfate, revealing that nitrate has a significant impact on the heterogeneous conversion of SO_2 to sulfate. The heterogeneous uptake of SO_2 on hematite is enhanced by a low to moderate amount of nitrate, and more sulfates are formed on hematite. For mixtures, the sample containing 24% nitrate exhibits the highest sulfate formation rate, and its corresponding uptake coefficient calculated by geometric surface area is about 5.5 times higher than that of hematite alone. The sample containing 48% nitrate presents the highest BET uptake coefficient, and the value is about 8 times higher than that of pure hematite. The enhanced formation of sulfate on particle surfaces and the change of particle surfaces would affect the hygroscopicity, optical properties and lifetime of the particle in the atmosphere. The observed formation of HONO and N_2O is of particular importance. The formation of potential HONO by this pathway may be significant for the conversion of SO_2 and the formation of sulfate in the atmosphere. The observed formation of N_2O may help to explain the difference between the sources of N_2O and the estimated sinks in the atmosphere and the observed increase in atmospheric N_2O. This study not only reveals the effects of nitrate on heterogeneous conversion of SO_2 on hematite but also provides new pathways for the formation of secondary sulfate aerosols, N_2O and potential HONO.

Results from this study have important atmospheric implications. Firstly, the results suggest that the heterogeneous conversion of SO_2 in the atmosphere will be affected by the availability of nitrate, and further emphasize that the complexity of the reaction of SO_2 on mineral dust. This chemistry may occur on surfaces of airborne dust particles that are known to be transported and play a role in the chemistry of the troposphere, which would affect the estimation of the amount of global atmospheric sulfate, and further

779 affect the previously estimated radiative forcing and cooling effect of sulfate aerosols in
780 the atmosphere (Dentener et al., 1996). Secondly, Fe (II) in airborne particles has been
781 observed (Zhu et al., 1997; Zhuang et al., 2001) and its concentration in dust increased
782 continuously during long-range transport (Zhuang et al., 2001). Also, in the real
783 atmospheric systems, sulfuric acid is a common component of particles (Finlayson-Pitts
784 and Pitts, 2000). $PM_{2.5}$ is generally acidic due to partial neutralization of acidic sulfate
785 and nitrate under some atmospheric conditions (Huang et al., 2011), and even dust
786 particle might become acidified to pH < 2 in the troposphere (Meskhidze et al., 2003).
787 The Fe (II)-containing airborne particles will inevitably be loaded by nitrate and be
788 acidified through contact with acidic particles such as sulfuric acid aerosols and acidic
789 $PM_{2.5}$ particles, or become the heterogeneous reaction interface of SO_2 and NO_2 in the
790 atmosphere. Hence, we can expect the production of potential HONO during these
791 processes. The results presented here may imply that such a heterogeneous conversion
792 pathway of low concentration SO_2 on nitrate-containing airborne dust particles may be a
793 potential and yet unknown daytime and nighttime significant source of HONO, and
794 reveal that the presence of nitrate on mineral dust aerosol may play a role in the
795 chemistry of HONO in the troposphere. In the meantime, these particles containing
796 potential HONO may become the oxidizing carriers for the oxidation of atmospheric
797 reduced gases, and thereby enhance the atmospheric oxidation ability. Understanding this
798 chemistry will contribute to the elucidation of the potential contribution of the unreleased
799 HONO in the particle for the conversion of SO_2 and the enhanced formation of sulfate in
800 the atmosphere in the daytime and at night. Finally, several studies indicated that the
801 photolysis of aqueous nitrate (Dubowski et al., 2001; Roca et al., 2008) and adsorbed

nitrate (Schuttlefield et al., 2008) is a source of NO_x (i.e., NO + NO_2), OH radicals and O (^3P). All of these products represent highly reactive oxidants in the gas phase and in other environmentally relevant phases. The production of hydroxyl radicals will favor the conversion of SO_2 to particulate sulfate, while the photolysis of aqueous or adsorbed nitrate will lead to a loss of nitrate in the particulate phase. Furthermore, according to our experimental results and discussion above, low to moderate amounts of nitrate will significantly promote the heterogeneous conversion of SO_2 and the formation of sulfate on airborne hematite-containing mineral dust particles, while the heterogeneous uptake of SO_2 on nitrate-containing mineral dust in the atmosphere will also bring a loss of adsorbed nitrate on the particle surface with the concomitant formation of gas-phase products including HONO and N_2O. Therefore, these studies mentioned above will aid in understanding the negative linear correlation between sulfate and nitrate contents in ambient particles (Kong et al., 2014). However, the reasons for the negative correlation are unknown. There is still lack of corresponding research on the formation mechanism of the negative correlation up to now, and all these aspects need to be further investigated.

Supplementary material related to this article is available online at

http://www.atmos-chem-phys-discuss.net/14/11577/2014/acpd-14-11577-2014-supplement.pdf.

Acknowledgements. This work was supported by the National Natural Science Foundation of China (Grant Nos. 21277028, 40775079, 21190053 and 41275126) and the

824 Scientific Research Foundation for the Returned Overseas Chinese Scholars, State
825 Education Ministry.

826 **References**

827 Ansari, A., Peral, J., Domènech, X., and Rodriquez-Clemente, R.: Oxidation of HSO_3^- in
828 aqueous suspensions of α-Fe_2O_3, α-FeOOH, β-FeOOH and γ-FeOOH in the dark and
829 under illumination, Environ. Pollut., 95, 283–288, 1997.

830 Arens, F., Gutzwiller, L., Baltensperger, U., Gäggler, H. W., and Ammann, M.:
831 Heterogeneous reaction of NO_2 on diesel soot particles, Environ. Sci. Technol., 35,
832 2191–2199, 2001.

833 Baltrusaitis, J., Cwiertny, D. M., and Grassian, V. H.: Adsorption of sulfur dioxide on
834 hematite and goethite particle surfaces, Phys. Chem. Chem. Phys., 9, 5542–5554, 2007.

835 Behra, P. and Sigg, L.: Evidence for redox cycling of iron in atmospheric water droplets,
836 Nature, 344, 419–421, 1990.

837 Börensen, C., Kirchner, U., Scheer, V., Vogt, R., and Zellner R.: Mechanism and kinetics
838 of the reactions of NO_2 or HNO_3 with alumina as a mineral dust model compound, J.
839 Phys. Chem. A, 104, 5036–5045, 2000.

840 Burley, J. D., and Johnston, H. S.: Ionic mechanisms for heterogeneous stratospheric
841 reactions and ultraviolet photoabsorption cross sections for NO_2^+, HNO_3, and NO_3^- in
842 sulfuric acid, Geophys. Res. Lett., 19, 1359–1361. 1992.

Chun, K. C. and Quon, J. E.: Capacity of ferric oxide particles to oxidize sulfur dioxide in air, Environ. Sci. Technol., 7, 532−538, 1973.

Dentener, F. J., Carmichael, G. R., Zhang, Y., Lelieveld, J., and Crutzen, P. J.: Role of mineral aerosol as a reactive surface in the global troposphere, J. Geophys Res., 101, 22869−22889, 1996.

Drescher, S. R. and Brown, S. D.: Solid phase microextraction-gas chromatographic–mass spectrometric determination of nitrous oxide evolution to measure denitrification in estuarine soils and sediments, J. Chromatogr. A, 1133, 300−304, 2006.

Dubowski, Y., Colussi, A. J., and Hoffmann, M. R.: Nitrogen dioxide release in the 302 nm band photolysis of spray-frozen aqueous nitrate solutions, Atmospheric implications, J. Phys. Chem. A, 105, 4928−4932, 2001.

EgashIra, M., NakashIma, M., KawasumI, S., and SeIyama, T.: Temperature programmed desorption study of water adsorbed on metal oxides. 2. Tin oxide surfaces, J. Phys. Chem., 85, 4125−4130, 1981.

Faguy, P. W. and Marinković, N. S.: An in situ infrared study on the effect of pH on anion adsorption at Pt (111) electrodes from acid sulfate solutions, Langmuir, 12, 243−247, 1996.

Finlayson-Pitts, B. J., and Pitts, J. N.: Chemistry of the upper and lower atmosphere: Theory, experiments, and applications, Academic Press, San Diego, CA, 2000.

862 Finlayson-Pitts, B. J., Wingen, L. M., Sumner, A. L., Syomin, D., and Ramazan, K. A.:
863 The heterogeneous hydrolysis of NO_2 in laboratory systems and in outdoor and indoor
864 atmospheres: An integrated mechanism, Phys. Chem. Chem. Phys., 5, 223–242, 2003.

865 Fu, H., Wang, X., Wu, H., Yin, Y., and Chen, J.: Heterogeneous uptake and oxidation of
866 SO_2 on iron oxides, J. Phys. Chem. C, 111, 6077–6085, 2007.

867 Goodman, A. L., Li, P., Usher, C. R., and Grassian, V. H.: Heterogeneous uptake of
868 sulfur dioxide on aluminum and magnesium oxide particles, J. Phys. Chem. A, 105,
869 6109–6120, 2001.

870 Goodman, A. L., Underwood, G. M., and Grassian, V. H.: A spectroscopic investigation
871 of the heterogeneous reaction $2NO_2 + H_2O$ (a) → HONO(g) + HNO_3 (a) on hydrated
872 silica Particles: Characterization of gas-phase and adsorbed products, J. Phys. Chem. A,
873 103, 7217–7223, 1999.

874 Harris, E., Sinha, B., van Pinxteren, D., Tilgner, A., Fomba, K. W., Schneider, J., Roth,
875 A., Gnauk, T., Fahlbusch, B., Mertes, S., Lee, T., Collett, J., Foley, S., Borrmann, S.,
876 Hoppe, P., and Herrmann, H.: Enhanced role of transition metal ion catalysis during in-
877 cloud oxidation of SO_2, Science, 340, 727–730, 2013.

878 Hixson, B. C., Jordan, J. W., Wagner, E. L., and Holly M.: Reaction products and
879 kinetics of the reaction of NO_2 with γ-Fe_2O_3, J. Phys. Chem. A, 115, 13364–13369,
880 2011.

881 Ho, K. F., Lee, S. C., Chan, C. K., Yu, J. C., Chow, J. C., and Yao, X. H.:
882 Characterization of chemical species in $PM_{2.5}$ and PM_{10} aerosols in Hong Kong, Atmos.
883 Environ., 37, 31–39, 2003.

884 Hoffman, R. C., Laskin, A., and Finlayson-Pitts, B. J.: Sodium nitrate particles: physical
885 and chemical properties during hydration and dehydration, and implications for aged
886 sea salt aerosols, J. Aerosol Sci., 35, 869–887, 2004.

887 Huang, X., Qiu, R., Chan, C. K., and Kant, P. R.: Evidence of high $PM_{2.5}$ strong acidity
888 in ammonia-rich atmosphere of Guangzhou, China: Transition in pathways of ambient
889 ammonia to form aerosol ammonium at $[NH_4^+]/[SO_4^{2-}]=1.5$, Atmos. Res., 99, 488–495,
890 2011.

891 Hug, S. J.: In situ Fourier transform infrared measurements of sulfate adsorption on
892 hematite in aqueous solutions, J. Colloid Interface Sci., 188, 415–422, 1997.

893 Hussain, G. and Rahman, M. M.: An infrared study of co-adsorption of N_2O and CO on
894 ZnO, Spectrochim. Acta, 64A, 880–885, 2006.

895 Jickells, T. D. and Spokes, L. J.: Atmospheric iron inputs to the ocean, in: the
896 biogeochemistry of iron in seawater, edited by: Turner, D. R. and Hunter, K. A.,
897 SCOR-IUPAC Series, J. Wiley, Baltimore, 85–121, 2001.

898 Kasibhatla, P., Chameides, W. L., and St John, J.: A three-dimensional global model
899 investigation of seasonal variations in the atmospheric burden of anthropogenic sulfate
900 aerosols, J. Geophys. Res., 102, 3737–3759, 1997.

Kerminen, V., Pirjola, L., Boy, M., Eskola, A., Teinilä, K., Laakso, L., Asmi, A., Hienola, J., Lauri, A., Vainio, V., Lehtinen, K., and Kulmala, M.: Interaction between SO_2 and submicron atmospheric particles, Atmos. Res., 54, 41–57, 2000.

Kleffmann, J., Gavriloaiei, T., Hofzumahaus, A., Holland, F., Koppmann, R., Rupp, L., Schlosser, E., Siese, M., and Wahner, A.: Daytime formation of nitrous acid: A major source of OH radicals in a forest, Geophys. Res. Lett., 32, L05818, doi: 10.1029/2005GL022524, 2005.

Kong, L., Yang, Y., Zhang, S., Zhao, X., Du, H., Fu, H., Zhang, S., Cheng, T., Yang, X., Chen, J., Wu, D., Shen, J., Hong, S., and Jiao, L.: Observations of linear dependence between sulfate and nitrate in atmospheric particles, J. Geophys. Res., 119, 341–361, 2014.

Laskin, A., Gaspar, D. J., Wang, W. H., Hunt, S. W., Cowin, J. P., Colson, S. D., and Finlayson-Pitts, B. J.: Reactions at interfaces as a source of sulfate formation in sea-salt particles, Science, 301, 340–344, 2003.

Lin, L., Kong, L., Chen, J., Experimental study of the effects of ammonium nitrate on SO_2 gas-particle transfer on the surface of atmospheric aerosols, Chem. J. Chinese U., 31, 751-755, 2010.

Liu, C., Ma, Q., Liu, Y., Ma, J., and He, H.: Synergistic reaction between SO_2 and NO_2 on mineral oxides: A potential formation pathway of sulfate aerosol, Phys. Chem. Chem. Phys., 14, 1668–1676, 2012.

921 Luria, M. and Sievering, H.: Heterogeneous and homogeneous oxidation of SO_2 in the
922 remote marine atmosphere, Atmos. Environ., 25, 1489–1496, 1991.

923 Martin, L. R., Damschen, D. E., and Judeikis, H. S.: The reactions of nitrogen oxides
924 with SO_2 in aqueous aerosols, Atmos. Environ., 15, 191–195, 1981.

925 McCurdy, P. R., Hess, W. P., and Sotiris S.: Nitric Acid-Water Complexes: Theoretical
926 Calculations and Comparison to Experiment, J. Phys. Chem. A, 106, 7628–7635, 2002.

927 Meskhidze, N., Chameides, W. L., Nenes, A., and Chen, G.: Iron mobilization in mineral
928 dust: Cananthropogenic SO_2 emissions affect ocean productivity?, Geophys. Res. Lett.,
929 30, 2085-2089, 2003.

930 Moore, J. K., Doney, S. C., Glover, D. M., and Fung, I. Y.: Iron cycling and nutrient-
931 limitation patterns in surface waters of the World Ocean, Deep Sea Res., Part II, 49 (1-
932 3), 463–507, 2002.

933 Nanayakkara, C. E., Pettibone, J., and Grassian, V. H.: Sulfur dioxide adsorption and
934 photooxidation on isotopically-labeled titanium dioxide nanoparticle surfaces: Roles of
935 surface hydroxyl groups and adsorbed water in the formation and stability of adsorbed
936 sulfite and sulfate, Phys. Chem. Chem. Phys., 14, 6957–6966, 2012.

937 Peak, D., Ford, R. G., and Sparks, D.: An in situ ATR-FTIR investigation of sulfate
938 bonding mechanisms on goethite, J. Colloid Interface Sci., 218, 289–299, 1999.

939 Persson, P. and Lovgren, L.: Potentiometric and spectroscopic studies of sulfate
940 complexation at the goethite-water interface, Geochim. Cosmochim. Ac., 60, 2789–
941 2799, 1996.

942 Pires, M., Van Den Bergh, H., and Rossi, M. J.: The heterogeneous formation of N_2O
943 over bulk condensed phases in the presence of SO_2 at high humidities, J. Atmos.
944 Chem., 25, 229–250, 1996.

945 Pires, M., Van Den Bergh, H., and Rossi, M. J.: The heterogeneous formation of N_2O in
946 the presence of acidic solutions: Experiments and modeling, Int. J. Chem. Kinet., 29,
947 869–891, 1997.

948 Pitts, J. N. Jr., Sanhueza, E., Atkinson, R., Carter, W. P. L., Winer, A. M., Harris, G. W.,
949 and Plum, C. N.: An investigation of the dark formation of nitrous acid in
950 environmental chambers, Int. J. Chem. Kinet., 16, 919–939, 1984.

951 Preszler Prince, A., Kleiber, P. D., Grassian, V. H., and Young, M. A.: Heterogeneous
952 interactions of calcite aerosol with sulfur dioxide and sulfur dioxide/nitric acid
953 mixtures, Phys. Chem. Chem. Phys., 9, 3432–3439, 2007.

954 Ramazan, K. A., Wingen, L. M., Miller, Y., Chaban, G. M., Gerber, R. B., Xantheas, S.
955 S., and Finlayson-Pitts, B. J.: New experimental and theoretical approach to the
956 heterogeneous hydrolysis of NO_2: Key role of molecular nitric acid and its complexes,
957 J. Phys. Chem. A, 110, 6886–6897, 2006.

Rivera-Figueroa, A. M., Sumner, A. L., and Finlayson-Pitts, B. J.: Laboratory studies of potential mechanisms of renoxification of tropospheric nitric acid, Environ. Sci. Technol., 37, 548−554, 2003.

Roca, M., Zahardis, J., Bone, J., El-Maazawi, M., and Grassian, V. H.: 310 nm irradiation of atmospherically relevant concentrated aqueous nitrate solutions: Nitrite production and quantum yields, J. Phys. Chem. A, 112, 13275–13281, 2008.

Schuttlefield, J., Rubasinghege, G., El-Maazawi, M., Bone, J., and Grassian, V. H.: Photochemistry of adsorbed nitrate, J. Am. Chem. Soc., 130, 12210−12211, 2008.

Schwertmann, U., and Cornell, R. M.: Iron oxides in the laboratory: Preparation and characterization, Wiley-VCH, New York, 2000.

Seinfeld, J. H. and Pandis, S. N.: Atmospheric Chemistry and Physics: From Air Pollution to Climate Change, 2nd edn., John Wiley & Sons Inc., New York, 2006.

Shi, Z., Bonneville, S., Krom, M. D., Carslaw, K. S., Jickells, T. D., Baker, A. R., and Benning, L. G.: Iron dissolution kinetics of mineral dust at low pH during simulated atmospheric processing, Atmos. Chem. Phys., 11, 995−1007, doi:10.5194/acp-11-995-2011, 2011.

Sugimoto, T. and Wang, Y.: Mechanism of the shape and structure control of monodispersed α-Fe_2O_3 particles by sulfate ions, J. colloid interface sci., 207, 137−149, 1998.

977 Summers, D. P.: Ammonia formation by the reduction of nitrite/nitrate by FeS: Ammonia
978 formation under acidic conditions, Origins Life Evol. B., 35, 299–312, 2005.

979 Ullerstam, M., Johnson, M. S., Vogt, R., and Ljungstrom, E.: DRIFTS and Knudsen cell
980 study of the heterogeneous reactivity of SO_2 and NO_2 on mineral dust, Atmos. Chem.
981 Phys., 3, 2043–2051, doi:10.5194/acp-3-2043-2003, 2003.

982 Ullerstam, M., Vogt, R., Langer, S., and Ljungström, E.: The kinetics and mechanism of
983 SO_2 oxidation by O_3 on mineral dust, Phys. Chem. Chem. Phys., 4, 4694–4699, 2002.

984 Underwood, G. M., Miller, T. M., and Grassian, V. H.: Transmission FT-IR and Knudsen
985 cell study of the heterogeneous reactivity of gaseous nitrogen dioxide on mineral oxide
986 particles, J. Phys. Chem. A, 103, 6184–6190, 1999.

987 Usher, C. R., Al-Hosney, H., Carlos-Cuellar, S., and Grassian, V. H.: A laboratory study
988 of the heterogeneous uptake and oxidation of sulfur dioxide on mineral dust particles, J.
989 Geophys. Res., 107, 4713–4721, 2002.

990 Usher, C. R., Michel, A. E., and Grassian, V. H.: Reactions on mineral dust, Chem. Rev.,
991 103, 4883–4939, 2003.

992 Watanabe, H., Gutleben, C. D., and Seto, J.: Sulfate ions on the surface of maghemite and
993 hematite, Solid State Ionics, 69, 29–35, 1994.

994 Wiesen, P., Kleffmann, J., Kurtenbach, R., and Becker, K. H.: Mechanistic study of the
995 heterogeneous conversion of NO_2 into HONO and N_2O on acid surfaces, Faraday
996 Discuss., 100, 121–127, 1995.

997 Wingen, L. M., Barney, W. S., Lakin, M. J., Brauers, T., and Finlayson-Pitts, B. J.: A
998 unique method for laboratory quantification of gaseous nitrous acid (HONO) using the
999 reaction HONO + HCl → ClNO + H_2O, J. Phys. Chem. A, 104, 329−335, 2000.

1000 Wu, L. Y., Tong, S. R., Wang, W. G., and Ge, M. F.: Effects of temperature on the
1001 heterogeneous oxidation of sulfur dioxide by ozone on calcium carbonate, Atmos.
1002 Chem. Phys., 11, 6593–6605, doi:10.5194/acp-11-6593-2011, 2011.

1003 Yamaguchi, T., Jin, T., and Tanabe, K.: Structure of acid sites on sulfur-promoted iron
1004 oxide, J. Phys. Chem., 90, 3148−3152, 1986.

1005 Zhang, Q. J., Wang, X., Chen, J. M., and Zhuang, G. S.: Formation of Fe (II) (aq) and
1006 sulfate via heterogeneous reaction of SO_2 with Fe_2O_3, Chem. J. Chinese U., 7, 1347−
1007 1350, 2007.

1008 Zhang, X., Zhang, G., Chen, J., Wang, Y., Wang, X., An, Z., and Zhang, P.:
1009 Heterogeneous reactions of sulfur dioxide on typical mineral particles, J. Phys. Chem.
1010 B, 110, 12588−12596, 2006.

1011 Zhu T., Shang J., and Zhao D. F.: The roles of heterogeneous chemical processes in the
1012 formation of an air pollution complex and gray haze, Sci. China Chem., 54, 145−153,
1013 2011.

1014 Zhu, X. R., Prospero, J. M., and Millero, F. J.: Diel variability of soluble Fe (II) and
1015 soluble total Fe in North African dust in the trade winds at Barbados, J. Geophys. Res.,
1016 102, 21297-21306, 1997.

1017 Zhuang, G., Yi, Z., Duce, R. A., and Brown, P. R.: Link between iron and sulphur cycles
1018 suggested by detection of Fe (II) in remote marine aerosols, Nature, 355, 537–539,
1019 1992.

1020 Zhuang, G. S., Guo, J. H., Yuan, H., and Zhao, C. Y.: The compositions, sources, and
1021 size distribution of the dust storm from China in spring 2000 and its impact on the
1022 global environment, Chinese Sci. Bull., 46, 895–901, 2001.

1023

1024

1025

1026

1027

1028

1029

1030

1031

1032

1033

1034

1035

1036

1037

1038 **Table 1.** Assignment of vibrational frequencies of surface species formed on hematite
1039 particle surfaces and on hematite-nitrate mixtures surfaces.

Surface species	Hematite (cm^{-1})	Hematite-nitrate mixture (cm^{-1})
SO_3^{2-}/HSO_3^-	1056	1080, 1050, 966
SO_4^{2-}	1361, 1337, 1261, 1158, 1056, 1000	1158, 1190, 987
Acidic species	1219	
NO_3^-		1599, 1587, 1567
NO_2^-		1506, 1487
Adsorbed HNO_3		1676, 1686, 1697, 1716
O-H region	3664, 3631	3664, 3631

1040

1041

1042

1043

1044

1045

Table 2. Sulfate formation rates and uptake coefficients for heterogeneous reactions of SO_2 on hematite and the hematite-nitrate mixtures at 298 K.

$NaNO_3$ (%)	A_{BET} (m^2/g)	Sulfate formation rate (ions s^{-1}) ($\times 10^{15}$)	$A_{geometric}$ (m^2) ($\times 10^5$)	γ_{BET} ($\times 10^7$)	$\gamma_{geometric}$ ($\times 10^3$)
0	12.1	1.28 ±0.07	7.85	5.58 ±0.29	2.58 ±0.14
2	11.8	1.48 ±0.15	7.85	6.60 ±0.69	2.98 ±0.31
4	11.7	2.01 ±0.12	7.85	9.04 ±0.56	4.04 ±0.25
6	11.5	3.62 ±0.18	7.85	16.6 ±0.81	7.29 ±0.35
12	10.9	4.93 ±0.29	7.85	23.8 ±0.14	9.93 ±0.58
24	9.1	7.11 ±1.34	7.85	41.2 ±0.78	14.3 ±2.69
48	5.2	4.39 ±0.39	7.85	44.5 ±0.39	8.84 ±0.78
60	4.0	1.62 ±0.25	7.85	21.3 ±0.32	3.25 ±0.49
72	2.8	0.59 ±0.15	7.85	11.2 ±0.29	1.19 ±0.31
90	1.3	0.15 ±0.03	7.85	6.10 ±1.05	0.30 ±0.05
100		0		0	0

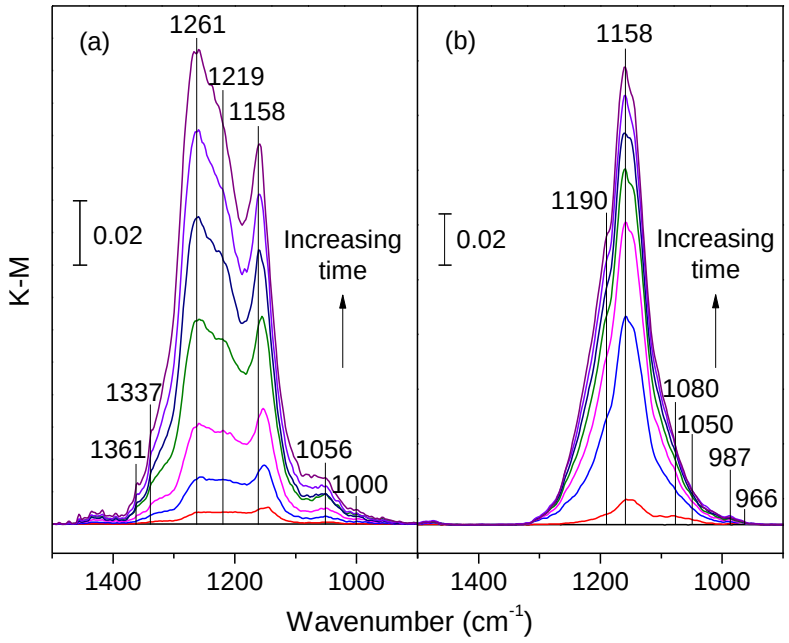

Fig. 1. DRIFT spectra of different samples recorded upon exposure to SO_2 at 298 K. **(a)** hematite. **(b)** FN-24.

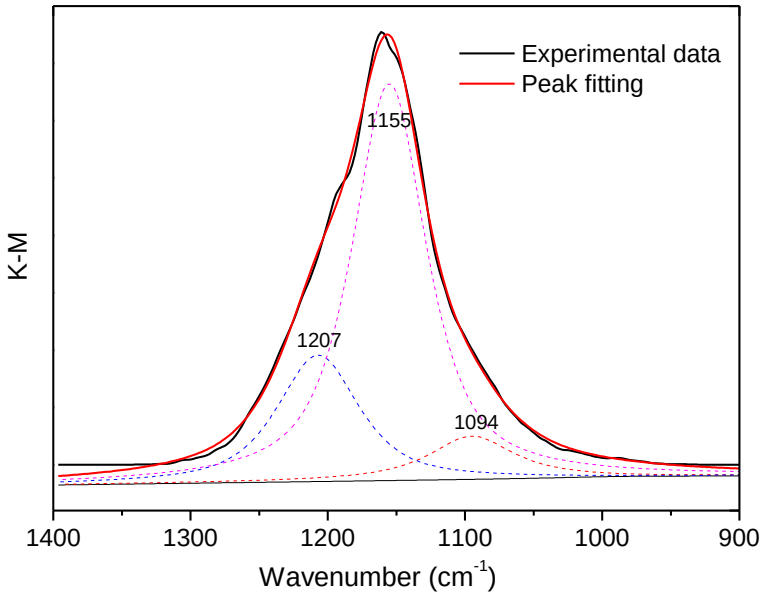

Fig. 2. Peak fitting of the last DRIFT spectrum of the products on FN-24 shown in Fig. 1 by mixed Gaussian-Lorentzian peak fitting.

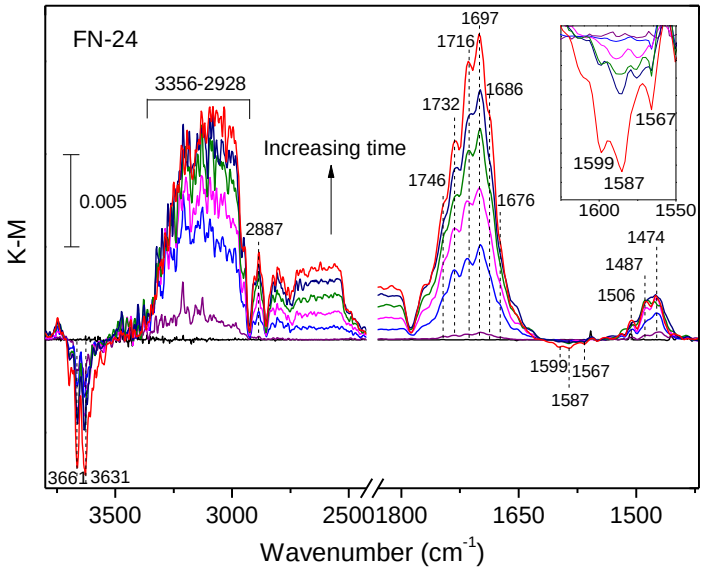

Fig. 3. DRIFT spectra of FN-24 as a function of time after exposure to SO_2 in the range of 3800 to 1350 cm^{-1}. The inset shows expanded region from 1630 to 1550 cm^{-1}.

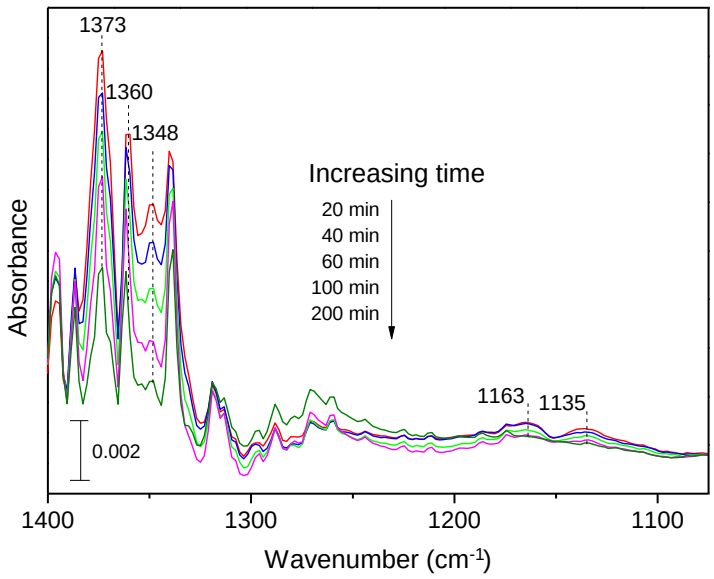

Fig. 4. In situ White cell-FTIR spectra of FN-24 recorded upon exposure to 50 ppm SO_2 + 21% O_2 at room temperature for different reaction times.

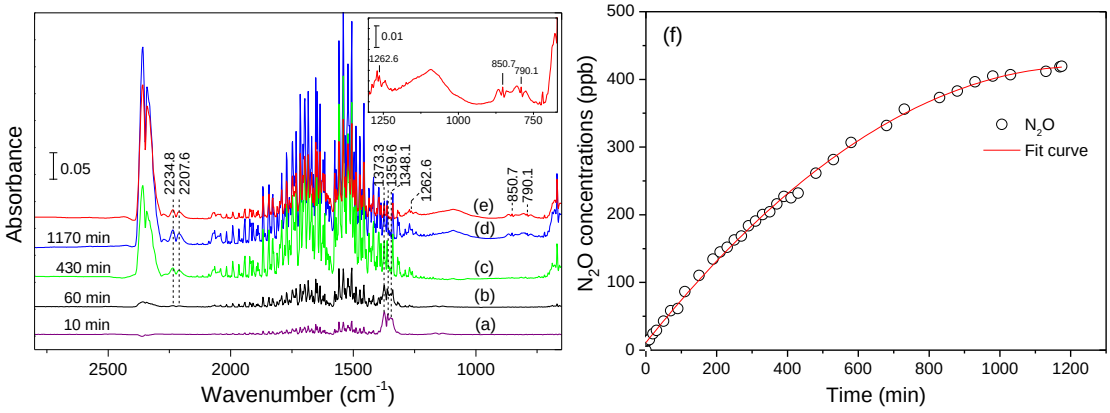

Fig. 5. In situ FTIR spectra of FN-90 recorded upon exposure to 12.5 ppm SO_2 + 21% O_2 at room temperature for different times. **(a)** 10 min. **(b)** 60 min. **(c)** 430 min. **(d)** 1170 min. **(e)** difference spectrum: (d) minus (c). **(f)** The concentration of the formed N_2O as a function of time during the reaction of FN-90 sample with SO_2.

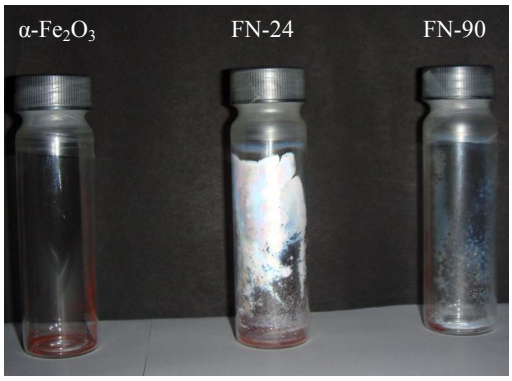

Fig. 6. Digital photos of different samples after reaction with 50 ppm SO_2 +21% O_2 in the dark at 298 K for about 7 days.

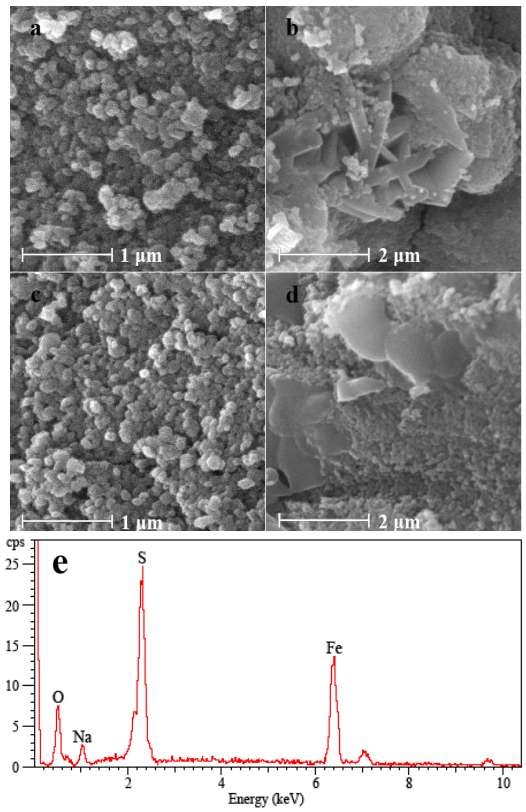

Fig. 7. SEM images and EDX spectrum. Top panels: SEM images of FN-24 **(a, b)** and FN-90 **(c, d)** particles before (left) and after (right) exposure to 3 ppm SO_2 at 298 K for 240 min. Bottom panel: typical EDX spectrum of the flaky substance.

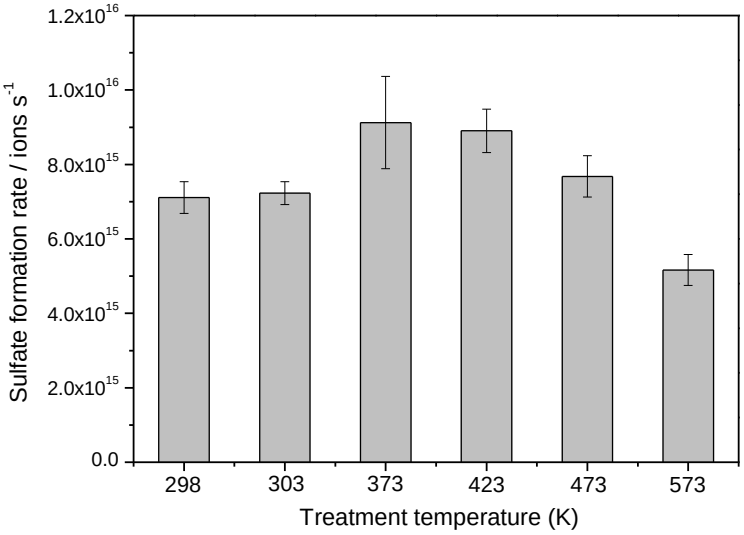

Fig. 8. Sulfate formation rates on 30 mg of FN-24 after exposure to 3 ppm SO_2 under different pre-treatment temperatures.

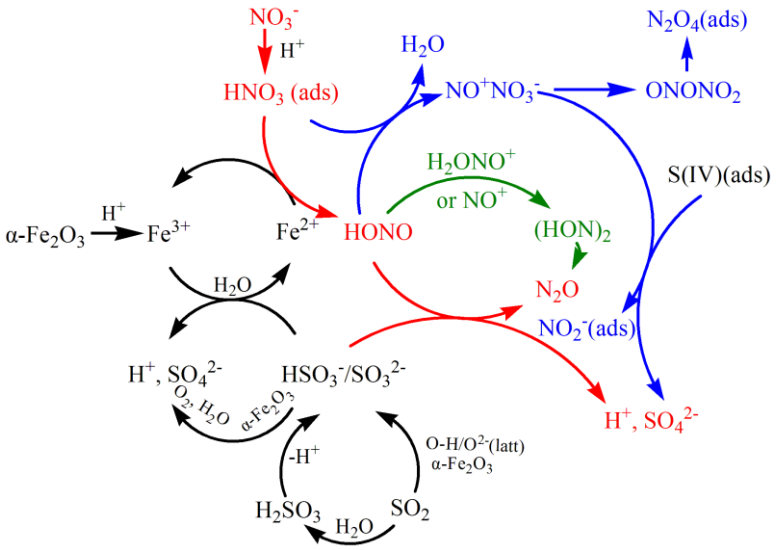

Fig. 9. Schematic of the reaction mechanism of the heterogeneous oxidation of SO_2 on hematite in the presence of nitrate.